Cavity Ring-Down Spectroscopy and Relative Rate Study of Reactions of HCO Radicals with O_2, NO, NO_2, and Cl_2 at 295 K

Yuki Ninomiya, Masashi Goto, Satoshi Hashimoto, Yoshihisa Kagawa, Kazunari Yoshizawa, and Masahiro Kawasaki*

Department of Molecular Engineering, Kyoto University, Kyoto 606-8501, Japan

Timothy J. Wallington and Michael D. Hurley

Ford Research Laboratory, SRL-3083, Ford Motor Company, Dearborn, Michigan 48121-2053

Received: March 29, 2000; In Final Form: June 1, 2000

Cavity ring-down absorption spectroscopy was used to measure $k(HCO + O_2) = (5.9 \pm 0.5) \times 10^{-12}$, $k(HCO + NO) = (1.9 \pm 0.2) \times 10^{-11}$, and $k(HCO + Cl_2) = (7.6 \pm 0.7) \times 10^{-12}$ cm^3 molecule^{-1} s^{-1} in 4−10 Torr of N_2 diluent at 295 K. FTIR/smog-chamber techniques were used to measure the following rate constant ratios in 15−750 Torr of N_2 diluent at 295K: $k(HCO + O_2)/k(HCO + Cl_2) = 0.85 \pm 0.02$, $k(HCO + NO)/k(HCO + Cl_2) = 2.80 \pm 0.10$, and $k(HCO + NO_2)/k(HCO + Cl_2) = 8.45 \pm 0.38$. Consistent results were obtained from the two different techniques. In 15−700 Torr of N_2 diluent at 295 K the reaction of HCO with Cl_2 proceeds via a single channel giving HC(O)Cl + Cl, reaction of HCO with NO gives CO in a yield indistinguishable from 100%, and reaction of HCO with NO_2 gives a 70% yield of CO and a 30% yield of CO_2. Ab initio calculations show that the reaction of HCO radicals with Cl_2 proceeds via the formation of the $HC(O)Cl_2$ complex, which decomposes, rapidly to HC(O)Cl and a Cl atom.

1. Introduction

The formyl radical is an important intermediate in the oxidation of organic compounds. Accurate kinetic and mechanistic data concerning HCO radicals are necessary to model the atmospheric and combustion chemistry of fossil fuels. Recognition of the importance of HCO radicals has led to numerous experimental and theoretical studies of its reactions with O_2,[1−11] NO[2−4,7−9,11], NO_2 [10,12−18], and Cl_2.[10]

$$HCO + O_2 \rightarrow HO_2 + CO \quad (1)$$

$$HCO + NO \rightarrow HNO + CO \quad (2)$$

$$HCO + NO_2 \rightarrow \text{products} \quad (3)$$

$$HCO + Cl_2 \rightarrow HC(O)Cl + Cl \quad (4)$$

As a result of these studies, the gross features of the kinetics and mechanisms of the above reactions are now clear. However, significant uncertainties persist in our understanding of the details of the above reactions. Reaction 1 is the most important fate of HCO radicals in the atmosphere and in combustion systems, and has been the subject of numerous kinetic studies. The NASA data evaluation panel[19] recommends use of $k_1 = 5.5 \times 10^{-12}$ cm^3 molecule^{-1} s^{-1} at 298 K in atmospheric models. However, recent measurements by Nesbitt et al.[11] suggest that a significantly lower value, $k_1 = 4.0 \times 10^{-12}$ cm^3 molecule^{-1} s^{-1} at 298 K, is more appropriate. In the modeling and interpretation of smog chamber data, accurate rate constant ratios for competing reactions are often more important inputs than the absolute rate constants themselves. There have been no measurements of the relative reactivites of O_2, NO, and NO_2 toward HCO radicals. There are considerable uncertainties in the absolute rate kinetic data for individual HCO reactions and relative reactivities of O_2, NO, and NO_2 derived from ratios of the absolute rate constant measurements carry substantial uncertainty. To clarify our understanding of HCO reaction kinetics and to establish the relative reactivities of O_2, NO, and NO_2, we have conducted kinetic studies of reactions 1−4 using a combination of cavity ring-down spectroscopy (CRDS)[20] and FTIR/smog chamber techniques.

CRDS is a new absorption technique based on measurement of the decay of a laser pulse confined within a cavity between two highly reflecting mirrors. Spectroscopic and kinetic data are derived by measuring the increased rate of decay of the laser pulse caused by absorption in the cavity.[21] The CRDS technique has been used in kinetic studies of phenyl,[22] vinoxy,[23] ethyl,[24] IO,[25] propargyl,[26] and BrO radicals.[27] The CRDS technique employs very long optical path lengths (1−20 km) and has greater sensitivity than conventional absorption techniques. The sensitivity of CRDS enables very low radical concentrations to be used, thus avoiding potential complications caused by radical−radical reactions. The initial HCO concentrations employed in the present study were $(1-2) \times 10^{12}$ cm^{-3}; a factor of 10−100 times lower than previous experiments employing conventional absorption techniques.[2,7−9]

The present work had two aims. First, to improve our understanding of the kinetics and mechanisms of reactions 1−4 under atmospheric conditions. Second, to extend the use of CRDS to the study of HCO radicals. As part of this work ab initio quantum mechanical calculations were performed to study the mechanism of the reaction of HCO radicals with Cl_2.

2. Experimental Section

The experimental systems used in this study are described in detail elsewhere.[27,28] Uncertainties reported herein are two

* E-mail: mkawasa7@ip.media.kyoto-u.ac.jp. Fax: +81-75-753-5526.

10.1021/jp001188b CCC: $19.00 © 2000 American Chemical Society
Published on Web 07/20/2000

standard deviations unless otherwise stated. Standard error propagation methods were used to combine uncertainties where appropriate.

2.1 The Cavity Ring-Down Spectroscopy System at Kyoto University. The CRDS apparatus is described in detail elsewhere.[27] A dye laser (Spectra Physics model PDL-3; fwhm = 0.1 cm^{-1}, sulforhodamine 640 dye) was pumped by the 532 nm output of a Nd:YAG laser (Quanta-Ray DCR-2) and injected into the ring-down cavity through one of the cavity end mirrors typically under 2 Hz operation. The mirrors (Research Electro Optics) had a diameter of 7.8 mm, a 1 m radius of curvature, and were mounted 1.04 m apart in PTFE disks connected to the glass flow tube by stainless steel bellows. Fine control of the mirror position was achieved using micrometer screws located alongside the bellows. The optical cavity had a ring down time of 50 μs at 613.5 nm. This ring-down time multiplied by the speed of light (3×10^8 m s^{-1}) gives an effective path length of 15 km. Light escaping from the ring-down cavity was detected by a photomultiplier tube (Hamamatsu R212UH) mounted behind one of the mirrors. Decay traces were recorded using a digital oscilloscope (Tektronix TDS430A) and transferred to a personal computer to calculate ring-down rates.

The ring-down cavity consisted of a glass tube (25 mm diameter) which was evacuated by a rotary pump and a mechanical booster pump with a liquid nitrogen trap. The pressure in the cell was monitored by an absolute pressure gauge (Baratron). The flows of sample gases were measured and regulated by mass flow controllers. A slow flow of nitrogen diluent was introduced at both ends of the ring-down cavity close to the mirrors to protect them from deposition of reaction products and reactants. Acetaldehyde (> 99%) was purified by freeze−pump−thaw cycling. Ultrahigh purity N_2, O_2, NO, and Cl_2 were used without further purification. Reaction mixtures consisted of 0.33−0.60 Torr ($1.1-1.9 \times 10^{16}$ cm^{-3}) CH_3CHO and 0−34 mTorr ($0-1.1 \times 10^{15}$ cm^{-3}) reactants (O_2, NO, or Cl_2) in 4−10 Torr total pressure of N_2 diluent at 295 ± 2 K. The samples in the cavity tube were completely refreshed for ≤ 2 Hz laser operation.

HCO radicals were produced by 266 nm pulsed laser photolysis of CH_3CHO:

$$CH_3CHO + h\nu\ (\lambda = 266\ \text{nm}) \rightarrow CH_3 + HCO \qquad (5)$$

HCO radicals were monitored by tuning the dye-laser on and off resonance with the head of R-branch in the $\tilde{A}^2A''(090) - \tilde{X}^2A'(000)$ band at 613.5−619 nm[29] (see the inset in Figure 1). The initial HCO concentration was $(1-2) \times 10^{12}$ cm^{-3}. The loss of HCO radicals via reactions 1, 2, and 4 was followed by variation of the delay time between the photolysis and probe laser pulses.

2.2 FTIR/Smog-Chamber System at Ford Motor Company. Experiments were performed in a 140-liter Pyrex reactor interfaced to a Mattson Sirus 100 FTIR spectrometer.[30] The reactor was surrounded by 22 fluorescent blacklamps (GE F15T8-BL) which were used to photochemically initiate the experiments. HCO radicals were produced by reaction of Cl atoms with HCHO. Cl atoms were generated by the photolysis of molecular chlorine in 15−700 Torr total pressure of N_2 diluent at 295 ± 2 K:

$$Cl_2 + h\nu \rightarrow 2Cl \qquad (6)$$

$$Cl + HCHO \rightarrow HCO + HCl \qquad (7)$$

Cl atoms were also formed via the reaction of HCO radicals with Cl_2. The loss of HCHO and formation of products were monitored by Fourier transform infrared spectroscopy using an infrared path length of 27.7 m, and a resolution of 0.25 cm^{-1}. Infrared spectra were derived from 32 co-added interferograms.

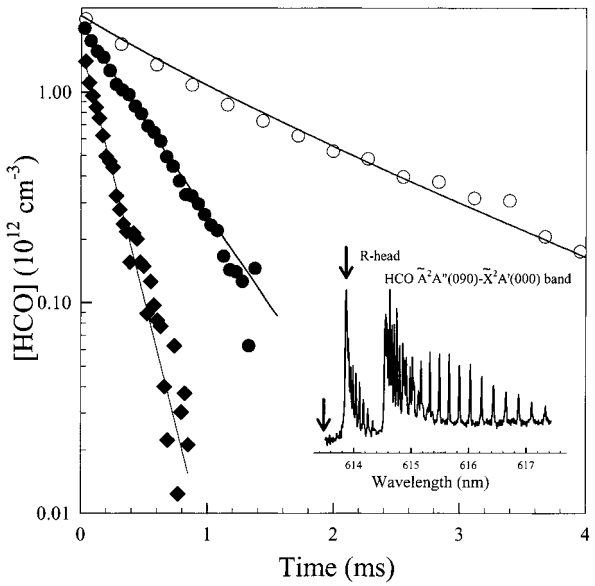

Figure 1. HCO decay following laser flash photolysis of mixtures containing 1.3×10^{16} cm^{-3} CH_3CHO in 4 Torr total pressure of N_2 diluent with $[O_2] = 0$ (○), 1.5×10^{14} (●), or 6.9×10^{14} cm^{-3} (◆). The lines are first-order fits. The inset shows the absorption spectrum of HCO. On- and off-resonance monitoring wavelengths are indicated by arrows.

Relative rate techniques were used to determine the rate constant ratios k_1/k_4, k_2/k_4, and k_3/k_4. Initial concentrations of the gas mixtures for the relative rate experiments were 7.1−13.2 mTorr HCHO, 0.35−1.12 Torr Cl_2, and either 0−21.2 Torr O_2, 0−3.48 Torr NO or 0−1.72 Torr NO_2 in 15−700 Torr N_2 diluent. NO and Cl_2 were obtained from commercial sources at purities >99% and used without further purification. Ultrahigh purity O_2 and N_2 were used as received. HCHO was prepared by heating paraformaldehyde powder and trapping the resulting HCHO vapor in a glass bulb using liquid nitrogen. NO_2 was prepared by mixing NO with excess O_2, waiting at least 1 h for the reaction of NO with O_2 to go to completion, freezing the mixture with liquid N_2, and pumping off the excess O_2.

In smog-chamber experiments, unwanted loss of reactants and products via photolysis, dark chemistry, and wall reactions have to be considered. Control experiments were performed to check for such unwanted losses of HC(O)Cl in 700 and 15 Torr of N_2 diluent. A slow, presumably heterogeneous, decomposition of HC(O)Cl into HCl and CO was observed with first-order loss rates of 2.3×10^{-3} and 3.6×10^{-3} min^{-1} in 700 and 15 Torr of N_2 diluent, respectively. On the time scale of the HCO kinetic experiments (5−15 min), heterogeneous loss of HC(O)Cl was negligible. Control experiments were performed to check for heterogeneous and/or photolytic loss of HCHO. Mixtures of HCHO in air diluent were left in the dark for 30 min then irradiated using all 22 blacklamps for 5 min; there was no observable (<2%) loss of HCHO.

3. Results

3.1 Kinetics of the Reactions of HCO with O_2, NO, and Cl_2 Investigated at Kyoto University. To study the kinetics of reactions 1, 2, and 4, the probe laser pulse was injected into the cavity at various delay times (0−9 ms) following the 266 nm photolysis of CH_3CHO in the presence of a reactant (O_2,

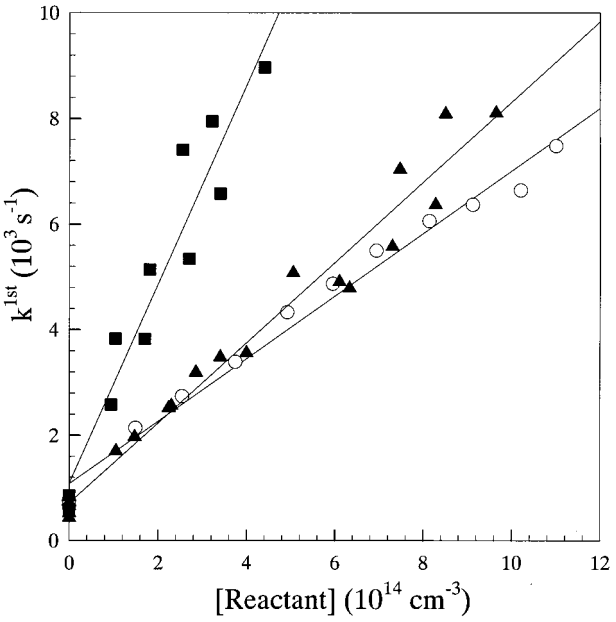

Figure 2. Plots of k^{first} versus the partial pressure of O_2 (circles), NO (squares), and Cl_2 (triangles). Data were obtained using the laser flash photolysis CRDS system.

NO, or Cl_2). In the presence of HCO radicals, the ring-down rate increased substantially reflecting absorption of the resonance dye laser radiation by HCO radicals in the cavity. The ring down rates, β, on and off resonance with the HCO absorption were recorded in back-to-back experiments at various delay times and the following formula was used to calculate the HCO radical concentrations:

$$\frac{(\beta_{on} - \beta_{off})L}{c} = (\sigma_{on} - \sigma_{off})\,[HCO]l \qquad \text{(i)}$$

where L is the cavity length (1.04 m), c is the speed of light, σ_{on} and σ_{off} are the absorption coefficients of HCO at the on and off resonance wavelengths, and "l" is the length of overlap between probe and photolysis laser pulses.

Results obtained using mixtures of 1.3×10^{16} cm^{-3} of CH_3CHO in 4 Torr total pressure of N_2 diluent with $[O_2] = 0$ (○), 1.5×10^{14} (●), or 6.9×10^{14} cm^{-3} (◆) are shown in Figure 1. As seen from Figure 1, the decay of HCO radicals followed first-order kinetics with rates which increased with increasing $[O_2]$. Linear least-squares analysis of the data in Figure 1 gives pseudo first-order loss rates, k^{1st}, for the loss of HCO radicals. Values of k^{1st} in the absence of added O_2 were 400−800 s^{-1} and are atttributed to diffusion and flow of HCO out of the viewing zone and loss of HCO via reaction with trace impurities of O_2. The recombination reaction of HCO radicals was considered to be negligible because the concentration of initially generated HCO radicals was low.

Figure 2 shows plots of the observed pseudo first-order loss rate of HCO radicals following photolysis of $CH_3CHO/O_2/N_2$, $CH_3CHO/NO/N_2$, or $CH_3CHO/Cl_2/N_2$ mixtures versus the partial pressure of O_2, NO, or Cl_2 in 4−10 Torr of N_2 diluent at 295 K. There was no observable effect of total pressure, over the range studied, on the kinetics of reactions 1, 2, and 4. Independent variation of the photolysis laser power (2.2−5.5 mJ/pulse), the repetition rate (1−10 Hz), and the initial concentration of HCO radicals had no discernible effect on the results. Linear least-squares analysis of the data in Figure 2 gives $k(HCO + O_2) = (5.9 \pm 0.5) \times 10^{-12}$, $k(HCO + NO) = (1.9 \pm 0.2) \times 10^{-11}$, and $k(HCO + Cl_2) = (7.6 \pm 0.7) \times 10^{-12}$ cm^3 molecule^{-1} s^{-1}.

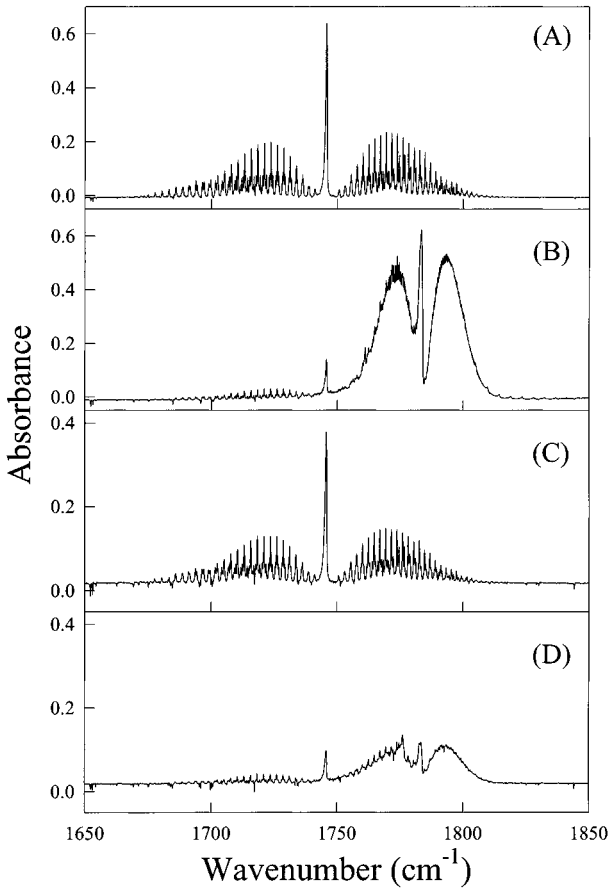

Figure 3. Infrared spectra acquired before (A) and after (B) a 4 s irradiation (2 fluorescent lamps) of a mixture of 12 mTorr of HCHO and 1.05 Torr of Cl_2 in 700 Torr of N_2. Panels C and D show spectra acquired before (C) and after (D) a 21 s irradiation (2 fluorescent lamps) of a mixture containing 7.7 mTorr HCHO, 1.05 Torr Cl_2, and 4.60 Torr O_2 in 700 Torr of N_2.

3.2 Relative Rate Study of the Reactions of HCO with O_2, NO, NO_2, and Cl_2 at Ford. Experiments were performed using the FTIR system at Ford to measure the rate constant ratios k_1/k_4, k_2/k_4, and k_3/k_4. The techniques used are described in detail elsewhere.[31] HCO radicals were generated by reaction of Cl atoms (produced by photolysis of Cl_2) with HCHO and allowed to react with either Cl_2 or one of the following: O_2, NO, or NO_2.

The reaction of HCO radicals with Cl_2 proceeds via one channel giving HC(O)Cl.[1] The rate constant ratios k_1/k_4, k_2/k_4, and k_3/k_4 were measured by monitoring the suppression of the HC(O)Cl yield following addition of known amounts of either O_2, NO, or NO_2 to $HCHO/Cl_2/N_2$ mixtures. Figure 3 shows typical spectra acquired before (A) and after (B) a 4 s UV irradiation (using 2 fluorescent lamps) of a mixture of 12 mTorr HCHO and 1.05 Torr Cl_2 in 700 Torr of N_2. The IR features in panel A are attributable to HCHO. The prominent product feature centered at 1763 cm^{-1} in panel B is caused by the formation of HC(O)Cl. Panels C and D show the results of an analogous experiment in which O_2 was present. In the presence of O_2 there is a competition between reactions 1 and 4 for the available HCO radicals. From a comparison of panels B and D it is clear that the addition of O_2 reduces the yield of HC(O)Cl. In a similar fashion it was observed that the presence of NO or NO_2 also reduced the HC(O)Cl yield.

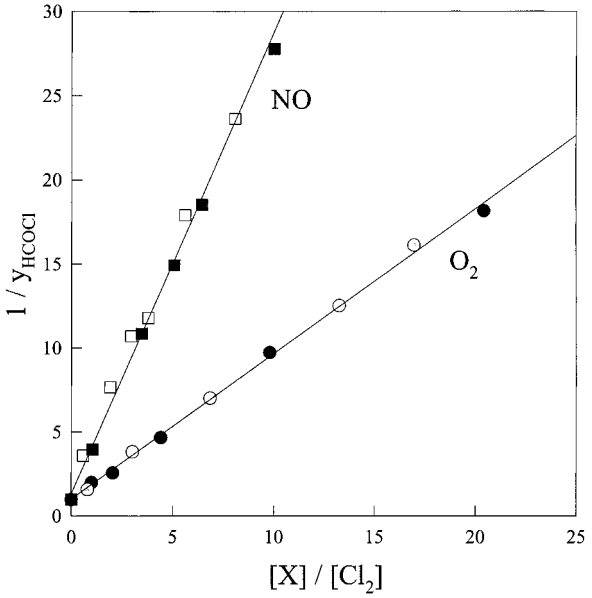

Figure 4. Plots of $1/y_{HCOCl}$ versus $[O_2]/[Cl_2]$ (circles) and $[NO]/[Cl_2]$ (squares) for experiments conducted in 15 (open), 50 (grey), or 700 Torr (filled symbols) of N_2 diluent. Data were obtained using the FTIR smog-chamber system.

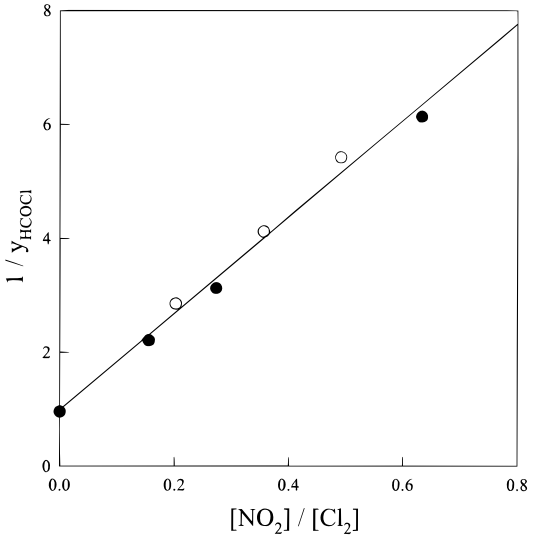

Figure 5. Plot of $1/y_{HCOCl}$ versus $[NO_2]/[Cl_2]$ for experiments conducted in 15 (open) or 700 (filled) Torr of N_2 diluent.

The yield of HCOCl, y_{HCOCl}, is related to the rate constant ratio k_x/k_4 by the expression (X = O_2, NO, or NO_2):

$$\frac{1}{y_{HCOCl}} = 1 + \frac{k_X}{k_4}\frac{[X]_0}{[Cl_2]_0} \qquad \text{(ii)}$$

where $[X]_0$ and $[Cl_2]_0$ are the initial concentrations of the reactants. Figures 4 and 5 show plots of the reciprocal of the HC(O)Cl yield versus the $[X]/[Cl_2]$ concentration ratio. In the presence of O_2, small amounts of formic acid product were observed. The formation of formic acid in such systems is well documented and originates from the slow reaction of HO_2 radicals with HCHO. In the calculation of y_{HCOCl} small (1−5%) corrections were made to the observed HCHO loss to account for loss via reaction with HO_2 radicals. Experiments were conducted in 15 (open symbols), 50 (grey symbols), or 700 Torr (filled symbols) of N_2 diluent. As expected from the expression above, the plots in Figures 4 and 5 are linear with

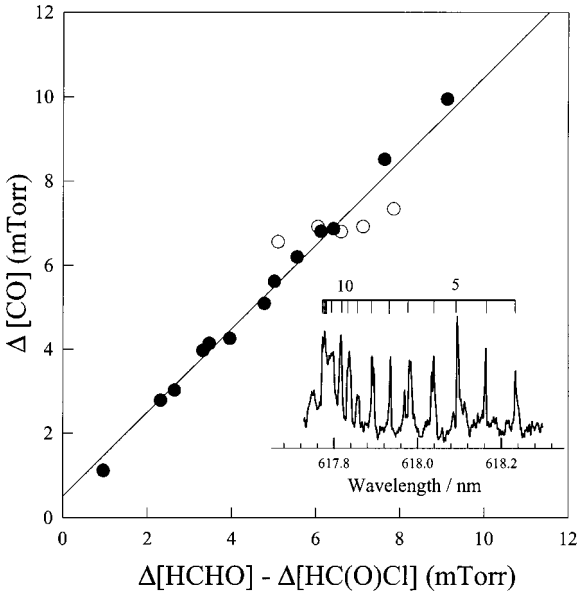

Figure 6. Plots of CO formation in the reaction of HCO radicals with NO determined using the FTIR smog-chamber technique. Experiments were performed in either 15 (open circles) or 700 Torr of N_2 diluent (filled circles). The inset shows the absorption spectrum of HNO in the region of the $\tilde{A}^1A''(100) - \tilde{X}^1A'(000)$ $^RR_3(J'')$ detected as a product of the HCO + NO reaction by CRD spectroscopy.

y-axis intercepts of unity. The slopes of such plots give the rate constant ratio k_x/k_4. Inspection of Figures 4 and 5 shows that there was no observable effect of total pressure over the range 15−700 Torr. Linear least-squares analysis of the data in Figures 3 and 4 gives $k_1/k_4 = 0.85 \pm 0.02$, $k_2/k_4 = 2.80 \pm 0.10$, and $k_3/k_4 = 8.45 \pm 0.38$.

3.3 Products of the Reactions of HCO with NO, NO_2, and Cl_2. The spectra acquired in the FTIR experiments described in the previous section contain information regarding the products of reactions (2−4). HC(O)Cl was the only carbon containing product observed following the UV irradiation of $HCHO/Cl_2/N_2$ mixtures at low (<40%) HCHO consumptions. For large HCHO consumptions we observe small amounts of CO produced by secondary reactions of Cl atoms with HC(O)Cl. These observations are entirely consistent with the previous determination by Niki et al.[32] that reaction 4 proceeds via one reaction channel, giving HC(O)Cl.

Two carbon containing products were observed following the UV irradiation of $HCHO/Cl_2/NO/N_2$ mixtures; HC(O)Cl and CO. The HC(O)Cl product is attributable to reaction 4, CO is a product of reaction 2. Figure 6 shows the observed CO formation versus HCHO loss (corrected for the fraction of the HCHO loss leading to HC(O)Cl formation) following UV irradiation of $HCHO/Cl_2/NO/N_2$ mixtures. Linear least-squares analysis gives a CO yield from the reaction of HCO radicals with NO of 103 ± 8%. The FTIR spectra were examined for evidence of HNO formation, but none was found. In the absence of a calibrated IR reference spectrum of HNO we are unable to deduce a product yield for this species from the FTIR experiments.

CRD spectroscopy experiments were performed to search for the formation of HNO. The characteristic visible absorption of HNO at 615−619 nm was observed following the laser flash photolysis of mixtures of 3.9 Torr CH_3CHO and 15 mTorr NO in 7.9 Torr N_2 diluent. The inset in Figure 6 shows the observed HNO spectrum which is assigned to the $\tilde{A}^1A''$ (100) − $\tilde{X}^1A'$ (000) transition.[33] While the CRD spectrum shown in the inset

TABLE 1: Kinetic Data for Reactions of HCO Radicals with O_2, NO, NO_2, and Cl_2 at 295 K

k(HCO + O_2) (10^{-12} cm^3 molecule^{-1} s^{-1})	k(HCO + NO) (10^{-11} cm^3 molecule^{-1} s^{-1})	k(HCO + Cl_2) (10^{-12} cm^3 molecule^{-1} s^{-1})	k(HCO + NO_2) (10^{-11} cm^3 molecule^{-1} s^{-1})	total pressure (Torr)	technique[a]	refs
5.7 ± 1.2				4 (He)	DF−PIMS	1
5.6 ± 0.9	0.85 ± 0.10			20−530 (He)	FP−VA	2
4.0 ± 0.8	1.4 ± 0.2			10 (HCHO)	LFP−IDLS	3
3.8 ± 1.0	1.2 ± 0.4			3−100 (N_2)	FP−IDLS	4
4.2 ± 0.7				4.2 (Ar)	FP−IDLS	5
5.1 ± 1.0				1−4 (He)	DF-LMR	6
4.6 ± 0.6	1.3 ± 0.2			3−1000 (N_2)	LFP-LRA	7
5.6 ± 1.2	1.2 ± 0.2			45−500 (N_2)	FP-LRA	9
			2.7 ± 0.9	3−58 (O_2)	LFP−PIMS	12
6.2 ± 1.2		7.1 ± 1.4	5.2	0.5−1.5 (He)	DF−PIMS	10
			5.7 ± 0.9	6−700 (SF_6)	LFP-LRA	15
4.0 ± 0.6	1.3 ± 0.2			1 (He)	DF−PIMS	11
5.9 ± 0.5	1.9 ± 0.2	7.6 ± 0.7		4−10 (N_2)	LFP−CRDS	this work−Kyoto
6.3 ± 1.5	2.1 ± 0.5	(7.4 ± 1.7)[b]	6.3 ± 1.5	15−700 (N_2)	FTIR−RR	this work−Ford

[a] DF = discharge flow, PIMS = photoionization mass spectrometry, FP = flash photolysis, VA = visible absorption, IDLS = intracavity dye laser spectroscopy, LMR = laser magnetic resonance, LRA = laser resonance absorption, CRDS = cavity ring down spectroscopy, FTIR−RR = Fourier transform infrared spectroscopy relative rate. [b] Value used to scale relative rate data.

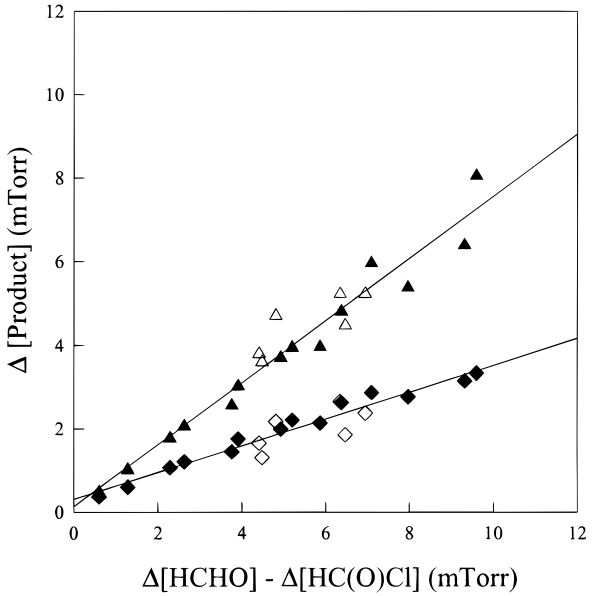

Figure 7. Plots of CO (triangles) and CO_2 (diamonds) formation in the reaction of HCO with NO_2. Experiments were performed in either 15 (open symbols) or 700 Torr of N_2 diluent (filled symbols). Data were obtained using the FTIR smog-chamber system.

in Figure 6 demonstrates that HNO is formed in the system, quantification of the HNO yield is not possible at this time. There are two possible sources of HNO that need to be considered: direct formation from HCO + NO and indirect formation via the H + NO reaction. Under our experimental conditions, the contribution of the latter process is negligibly small, since H atoms generated by 266 nm photolysis of CH_3CHO are efficiently scavenged by reaction with CH_3CHO and not with NO. The observed HNO is a product of reaction 2.

Three carbon containing products were observed following UV irradiation of HCHO/Cl_2/NO_2/N_2 mixtures: HC(O)Cl, CO, and CO_2. The triangles and diamonds in Figure 7 show the observed CO and CO_2 formation versus HCHO loss following the UV irradiation of HCHO/Cl_2/NO_2/N_2 mixtures. The HCHO loss is corrected for the fraction of HCHO loss that leads to HC(O)Cl formation. Linear least-squares analysis of the data in Figure 7 gives a 74 ± 9% CO yield and a 32 ± 6% CO_2 yield. Normalizing the combined CO and CO_2 yields from the present work to 100% we arrive at branching ratios of (k_{3a} + k_{3b})/(k_{3a} + k_{3b} + k_{3c} + k_{3d}) = 0.70 ± 0.08 and (k_{3c} + k_{3d})/(k_{3a} + k_{3b} + k_{3c} + k_{3d}) = 0.30 ± 0.05 in 15−700 Torr of N_2 diluent at 295 K:

TABLE 2: Reported Branching Ratios for Reaction 3

(3a)	(3b)	(3c)	(3d)	ref
			∼1	12
0.66	0	0	0.34	13
0.79	0	0	0.21	14
0.48 ± 0.14	0	0.52 ± 0.14:3c < 0.10		15
<0.05	0.63 ± 0.05	0.05	0.37 ± 0.05	16
0.62		0	0.38	17
0.66 ± 0.10	0		0.34 ± 0.10	18
0.70 ± 0.08		0.30 ± 0.05		this work

	ΔH°_{298} (kcal mol^{-1})	
HCO + NO_2 → CO + HONO	−63.3	(3a)
→ CO + OH + NO	−13.5	(3b)
→ CO_2 + HNO	−86.4	(3c)
→ CO_2 + H + NO	−38.3	(3d)

As indicated above, it is expected that HONO and/or NO will be formed as products in reaction 3. HONO and NO were indeed detected in the FTIR experiments. However, the formation of these species via processes unrelated to reaction 3, i.e., reaction with H_2O on the chamber walls and photolysis of NO_2, precludes a reliable estimate of their product yields from reaction 3. As seen from Table 2, with the exception of the results from Guo et al.,[15] our measured CO and CO_2 yields are consistent with the mechanistic findings of previous workers. In the absence of product data for HONO, HNO, or NO from the FTIR experiments, it is not possible to distinguish between channels 3a and 3b, or between 3c and 3d.

3.4 Ab Initio Study of the Mechanism of the HCO + Cl_2 Reaction. Rate constants for the reaction of HCO + Cl_2 at 295 K were calculated. Reactant, transition state, intermediate, and product geometries were optimized at the density functional theory (DFT) using the unrestricted Becke[34] three-parameter hybrid method with the Lee, Yang, and Parr[35] correlation functional and the 6-311G(d,p) basis set[36] (denoted as B3LYP/6-311G(d,p)). Vibrational frequency analyses were also carried out at the same level of theory. To confirm the reliability of the DFT calculations, single-point energy calculations were performed at the QCISD(T) level with the 6-311G(d,p) basis set using the B3LYP optimized geometries. As shown in Figure 8, the computed energy values at the B3LYP level are in good

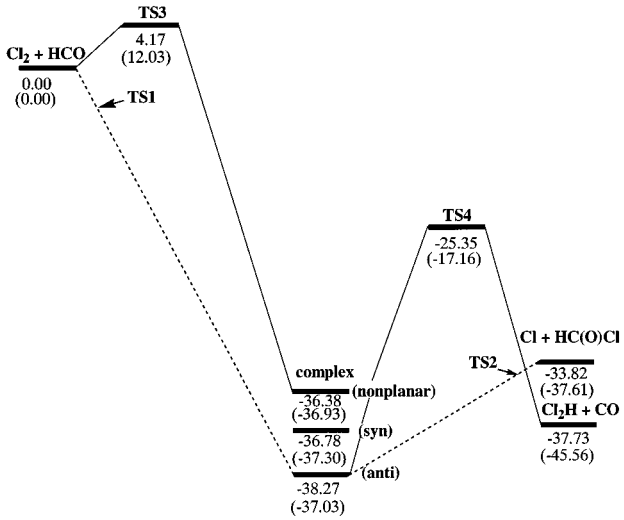

Figure 8. Potential energy surface at the B3LYP/6-311G(d,p) level of theory (without ZPE correction). The values in parentheses correspond to the QCISD(T)/6-311G(d,p) level. Relative values are in kcal mol^{-1}.

agreement with those at the QCISD(T) level. Therefore, we are able to derive reasonable results from the energies and the vibrational frequencies computed at the B3LYP level of theory for the entire rate calculations shown below. Transition states were subjected to intrinsic reaction coordinate (IRC) calculations to facilitate a connection with minima along the reaction pathways.[37] Our IRC analyses identified the true local minimum points. All ab initio calculations were performed with the Gaussian 94 program package.[38]

Three possible pathways were found for the reaction HCO + Cl_2. The optimized geometries of various reaction species involved in these pathways are shown in Figure 9. The profile of the potential energy surface at the B3LYP/6-311G-(d,p) level is shown in Figure 8. In the first pathway, the reaction starts with the attachment of Cl_2 to the carbon atom of HCO to form the $HC(O)Cl_2$ complex, in which the Cl−Cl bond is almost cleaved. Three local minimum points for the $HC(O)Cl_2$ complex with the syn-, anti-, and nonplanar structures were found, but there is little energy difference ($\leq$ 2 kcal mol^{-1}) among these stereoisomers at both B3LYP and QCISD(T) levels of theory. Therefore, among these thermodynamically equivalent structures, we employed the antistructure that has the lowest potential energy at the B3LYP level of theory. This complex dissociates into HC(O)Cl + Cl via TS2 located on the potential energy surface along the reaction coordinate, the Cl···Cl distance. Because of the absence of van der Waals interaction between the Cl radical and the HC(O)Cl species, the products are 3.91 kcal mol^{-1} less stable than the complex at the B3LYP level. The Cl···Cl bond of the complex has a length of 2.846 Å and is almost cleaved. The $HC(O)Cl_2$ complex has an excess internal energy resulting from the large binding energy of formyl radical and molecular chlorine, and hence, it can easily decompose to

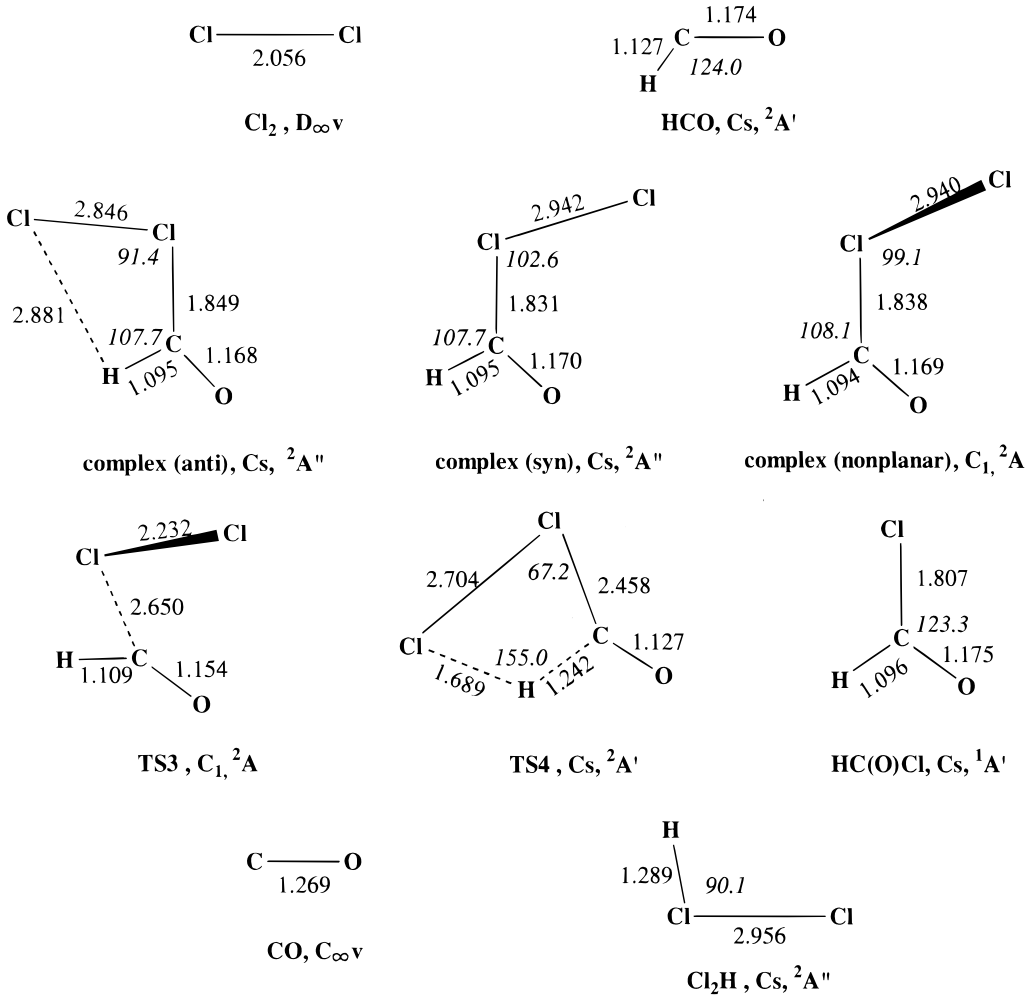

Figure 9. B3LYP/6-311G(d,p) optimized geometries of the reactants, products, various intermediates, and transition states (TS) for the Cl_2 + HCO reaction.

HC(O)Cl and a Cl atom. In the second pathway, the complex dissociates into Cl_2H + CO via TS4. In this pathway, Cl_2 abstracts the H atom of the formyl group via the four-centered transition state, TS4, to form Cl_2H. This pathway gives products, Cl_2H + CO, that are slightly more stable than Cl + HC(O)Cl. The high activation barrier (12.92 kcal mol^{-1} at the B3LYP level and 19.87 kcal mol^{-1} at the QCISD(T) level) implies, however, that the second pathway is unlikely to occur compared with the first one. In the third pathway, the Cl atom of molecular chlorine is abstracted via TS3. In the course of this reaction, the molecular chlorine attacks the formyl radical within C_1 symmetry, giving a nonplanar complex. This stereochemical feature is different from the first and the second pathways, in which the whole reaction proceeds keeping C_s symmetry.

Simple transition state theory (TST) was used to calculate the rate constants for the entrance channel of the first and third pathways. In the first and second pathways, which are identical with respect to the first half of the reaction, the formation of the complex from the reactants passes through TS1 with almost no cost of energy because of the high reactivity of the radical species. Therefore, we used the "loose transition state" model,[39] which is widely used to model the kinetics for many barrierless reactions to determine the rate constant for this process. According to this simple but useful method, the rate constant expressed in cm^3 $molecule^{-1}$ s^{-1} takes the form

$$k(T) = \alpha\left(\frac{g^{\ddagger}}{g_{HCO}g_{Cl_2}}\right)\left(\frac{h^3}{k_B T}\right)\left(\frac{ABCI_D}{A'B'C'I_{Cl_2}}\right)\left(\frac{m^{\ddagger}}{m_{HCO}m_{Cl_2}}\right)^{2/3} Q_{vib} \quad \text{(iii)}$$

where $g^{\ddagger}$, g_{CHO}, and g_{Cl_2} are the electronic multiplicities of the loose transition state and of the reactants, respectively. Q_{vib} is the ratio of vibrational partition functions of the transition state and the reactants. A, B, and C are the moments of inertia (g cm^2) of the transition state. A', B', and C' are the moments of inertia of HCO. I_{Cl_2} is the moment of inertia of Cl_2, and I_D is the reduced moment of inertia for rotation around the C···Cl bond. Also, $m^{\ddagger}$ and m_i are the masses of the transition state and the reactants, in grams, and α includes the reaction symmetry number and the numerical coefficient, resulting from the approximation of the harmonic oscillator to the internal free rotor. The geometric structure of such a transition state can be described with the Gorin model,[40] assuming that the C···Cl distance in TS is 3.5 times larger than the C···Cl distance in the complex and holding constant the structural parameters for Cl_2 and HCO. The calculated rate constant of the first and second pathways is 1.0×10^{-11} cm^3 $molecule^{-1}$ s^{-1} at 295 K. On the other hand, the rate constant for the third pathway that passes through TS3 is 2.3×10^{-16} cm^3 $molecule^{-1}$ s^{-1} at 295 K. This small rate constant compared with those of the first and second pathways shows that the third pathway can be neglected.

RRKM calculations using the following mechanism were conducted to evaluate the total rate constant for the first and second pathways:

$$\begin{aligned} HCO + Cl_2 \underset{b}{\overset{a}{\rightleftarrows}} (HCO(O)Cl_2)^* &\xrightarrow{c} Cl_2H + CO \\ &\xrightarrow{d} HC(O)Cl + Cl \\ &\xrightarrow{e} HC(O)Cl_2(+M) \end{aligned} \quad \text{(iv)}$$

In this reaction, $(HC(O)Cl_2)^*$ represents the vibrationally excited intermediate, and step (e) is a collisional relaxation process. The rate constants for the disappearance of HCO into various products can be evaluated on the basis of the RRKM theory[41]

$$k_i = l_a \frac{k_B T}{h} \frac{Q_t^{\ddagger} Q_r^{\ddagger}}{Q_{HCO} Q_{Cl_2}} e^{-E_a/RT} \int_0^{\infty} \frac{k_i(E) \sum P_a(E_a^{\ddagger}) e^{-E_a^{\ddagger}/RT}}{\sum k_i(E) + \omega} \frac{dE_a^{\ddagger}}{RT} \quad \text{(v)}$$

$$k_e = l_a \frac{k_B T}{h} \frac{Q_t^{\ddagger} Q_r^{\ddagger}}{Q_{HCO} Q_{Cl_2}} e^{-E_a/RT} \int_0^{\infty} \frac{\omega \sum P_a(E_a^{\ddagger}) e^{-E_a^{\ddagger}/RT}}{\sum k_i(E) + \omega} \frac{dE_a^{\ddagger}}{RT} \quad \text{(vi)}$$

$$k_i(E) = C_i \sum P_i(E_i^{\ddagger})/hN(E) \quad \text{(vii)}$$

$$\omega = \beta_c Z_{LJ}\,[M] \quad \text{(viii)}$$

where $i = b$, c, and d, and l_a is the reaction path degeneracy for the formation of $(HC(O)Cl_2)^*$ via step (a). Q_{HCO} and Q_{Cl_2} are the total partition functions of HCO and Cl_2, respectively. $Q_t^{\ddagger}$ and $Q_r^{\ddagger}$ are the translational and rotational partition functions of TS1 for step (a), respectively. That transition state has an energy barrier E_a at 0 K. However, as mentioned above, E_a is practically zero, $k_i(E)$ is the energy-specific rate constant for step (i), and C_i is the product of the statistical factor and the ratio of overall rotational partition function of the transition state for step (i) to the complex, $HC(O)Cl_2$. $\Sigma P_a(E_a^{\ddagger})$ is the sum of states of the transition state for step (a) with excess energy $E_a^{\ddagger}$, and $N(E)$ is the density of states of $(HC(O)Cl_2)^*$ having a total energy E, ω is the effective collision frequency for the deactivation of $(HC(O)Cl_2)^*$ via step (e), and β_c is the collision efficiency, which is calculated by Troe's weak-collision approximation.[42] Z_{LJ} is the Lennard-Jones collision frequency. In this calculation, we used the following parameters: the temperature-dependent collisional efficiency $\beta_c = 0.48 - 0.60$, the energy dependent factor of the density of state $F_E = 1$, the Lennard-Jones potential collisional diameter $\sigma = 0.445$ nm and the Lennard-Jones well depth $\epsilon/k_B = 144$ K.[43]

The experimentally observed rate constant of HCO + Cl_2 (k_4), is reproduced as follows:

$$k_4 = k_c + k_d + k_e \quad \text{(ix)}$$

The calculated temperature and pressure dependence of the total rate constant were k_4 (T, P = 4 Torr of N_2) = 1.0×10^{-11} to 8.8×10^{-12} cm^3 $molecule^{-1}$ s^{-1} for T = 340−200 K and k_4 (T = 295 K, P) = 1.0×10^{-11} cm^3 $molecule^{-1}$ s^{-1} for P = 1−760 Torr of N_2. Our calculations show that the total rate constant k_4 is independent of pressure. The calculated rate constant was entirely consistent with the experimental findings. In this temperature and pressure range, k_d was much larger than k_b, k_c, and k_e. The results show that step (d) is the major (> 99.56%) channel of this reaction.

The ab initio study showed that reaction of HCO radicals proceeds via the formation of the $HC(O)Cl_2$ complex, which possesses significant internal excitation and decomposes essentially immediately to give HC(O)Cl and Cl. Hsu et al.[44] calculated k_3 at the same level of theory. Comparing their value with ours gives $k_1/k_4 = 0.68$, which is consistent, within the accuracy of the calculations, with our experimental determination of $k_1/k_4 = 0.85 \pm 0.02$.

4. Discussion

The results from the present work are compared to the previous data in Table 1. The value of $k_4 = (7.6 \pm 0.7) \times 10^{-12}$ cm^3 mol^{-1} s^{-1} measured using the CRDS technique in the

present work is in excellent agreement with the previous determination of $k_4 = (7.1 \pm 1.4) \times 10^{-12}$ cm^3 molecule^{-1} s^{-1} by Timonen et al.[10] These values are consistent with the calculated result of $k_4 = 1.0 \times 10^{-11}$ cm^3 molecule^{-1} s^{-1} in the present work. Averaging the two experimental determinations gives $k_4 = (7.4 \pm 1.7) \times 10^{-12}$ cm^3 molecule^{-1} s^{-1} (error limits encompass extremes of both determinations) which, combined with the rate constant ratios $k_1/k_4 = 0.85 \pm 0.02$, $k_2/k_4 = 2.80 \pm 0.10$, and $k_3/k_4 = 8.45 \pm 0.38$, give $k_1 = (6.3 \pm 1.5) \times 10^{-12}$, $k_2 = (2.1 \pm 0.5) \times 10^{-11}$, and $k_3 = (6.3 \pm 1.5) \times 10^{-11}$ cm^3 molecule^{-1} s^{-1}. The CRDS and FTIR techniques provide a consistent picture of the behavior of HCO radicals.

As seen from Table 1, the reactivity of HCO radicals toward NO_2 measured here is in good agreement with the previous results of Guo et al.[15] and Timonen et al.,[10] but is approximately a factor of 2 higher than reported by Morrison and Heicklen.[12] For reasons which are unclear, it appears that Morrison and Heicklen underestimated the rate of reaction 3.

Reported values of k_1 fall in two broad groups with k_1 values of approximately 4×10^{-12} [3-5,11] or 6×10^{-12} cm^3 molecule^{-1} s^{-1}.[1,2,6,9,10] The results from our CRDS and relative rate studies are consistent with the latter. As noted by Veyret and Lesclaux[9] and the NASA data panel,[19] three out of the four measurements giving $k_1 = 4 \times 10^{-12}$ were performed using static systems in which reaction mixtures were subjected to multiple photolysis pulses.[3-5] Veyret and Lesclaux[9] showed that multiple photolysis pulses on a static reaction mixture lead to a significant consumption of O_2 and an underestimation of k_1. Accordingly, we will not consider the results from refs 3−5 further. Nesbitt et al.[11] used a discharge flow system recently to measure $k_1 = (4.0 \pm 0.6) \times 10^{-12}$ cm^3 molecule^{-1} s^{-1}, consumption of O_2 is not a problem in such a discharge flow study. It is difficult to understand why the value of k_1 reported by Nesbitt et al. appears to be anomalously low. Taking an average of the measurements of k_1 listed in Table 1, including the two determinations reported herein (but excluding ref 3−5), gives $k_1 = 5.4 \times 10^{-12}$ cm^3 molecule^{-1} s^{-1} which we recommend for use in models to describe the chemistry occurring in smog-chamber experiments designed to simulate atmospheric reactions. The value of $k_1 = 6.8 \times 10^{-12}$ cm^3 molecule^{-1} s^{-1} calculated by Hsu et al.[44] is consistent with our experimental data.

Finally, we need to consider the kinetic data for the reaction of HCO radicals with NO. Initial inspection of the existing database for k_2 (see Table 1) suggests that the kinetics of this reaction are well established. As shown in Table 1, there have been six previous measurements of k_2, and with one exception (Shibuya et al.[2]), the agreement between all published data is excellent. However, a closer inspection of the published work reveals that the database for k_2 is not as compelling as it seems. First, as discussed above, the work of Reilly et al.[3] and Nadtochenko et al.[4] may underestimate k_2 because of consumption of NO reactant by multiple photolysis pulses on a static reaction mixture. Second, Reilly et al.[3] reported that HNO product was formed significantly faster than HCO reactant was lost and stated that "if anything the value of k_2 is larger than the value reported" in their work. Third, because of the unexpected observation that NO was not consumed in control experiments employing multiple flashes on static mixtures, Veyret and Lesclaux[9] state that "the reliability of the k_{NO} value is not as good as for k_{O2}" in their study. At the present time we are unable to explain the 50% discrepancy between our measured value for k_2 and the previous determinations.

Acknowledgment. We thank the Japanese Government for a NEDO grant which made this collaborative research project possible, Gus Hancock (University of Oxford), Andrew J. Orr-Ewing (University of Bristol), and Bill Schneider (Ford) for helpful comments, and Kenichi Tonokura (University of Tokyo) for his help in calculation of the rate constants.

Note Added in Proof. Yamazaki et al.[45] have reported $k(HCO + O_2) = (6.6 \pm 0.3) \times 10^{-12}$ cm^3 mol^{-1} s^{-1} using a laser-induced fluorescence method. This result is consistent with our findings.

References and Notes

(1) Washida, N.; Martinez, R. I.; Bayes, K. D. *Z. Naturforsch. A.* **1974**, *29*, 251.
(2) Shibuya, K.; Ebata, T.; Obi, K.; Tanaka, I. *J. Phys. Chem.* **1977**, *81*, 2292.
(3) Reilly, J. P.; Clark, J. H.; Moore, C. B.; Pimentel, G. C. *J. Chem. Phys.* **1978**, *69*, 4381.
(4) Nadtochenko, V. A.; Sarkisov, O. M.; Vedeneev, V. I. *Dokl. Akad. Nauk SSSR* **1979**, *244*, 152.
(5) Gill, R. J.; Johnson, W. D.; Atkinson, G. H. *Chem. Phys.* **1981**, *58*, 29.
(6) Temps, F.; Wagner, H. Gg. *Ber. Bunsen Ges. Phys. Chem.* **1984**, *88*, 410.
(7) Langford, A. O.; Moore, C. B. *J. Chem. Phys.* **1984**, *80*, 4204.
(8) Langford, A. O.; Moore, C. B. *J. Chem. Phys.* **1984**, *80*, 4211.
(9) Veyret, B.; Lesclaux, R. *J. Phys. Chem.* **1984**, *85*, 1918.
(10) Timonen, R. S.; Ratajczak, E.; Gutman, D. *J. Phys. Chem.* **1988**, *92*, 651.
(11) Nesbitt, F. L.; Gleason, J. F.; Stief, L. J. *J. Phys. Chem. A* **1999**, *103*, 3038.
(12) (a) Morrison, B. M., Jr.; Heicklen, J. *J. Photochem.* **1980**, *13*, 189. (b) Morrison, B. M., Jr.; Heicklen, J. *J. Photochem.* **1981**, *15*, 131.
(13) He, Y.; Kolby, E.; Shumaker, P.; Lin, M. C. *Int. J. Chem. Kinet.* **1989**, *21*, 1015.
(14) Lin, C.-Y.; Wang, H.-T.; Lin, M. C.; Melius, C. F. *Int. J. Chem. Kinet.* **1990**, *22*, 455.
(15) Guo, Y.; Smith, S. C.; Moore, C. B.; Melius, C. F. *J. Phys. Chem.* **1995**, *99*, 7473.
(16) Rim, K. T.; Hershberger, J. F. *J. Phys. Chem. A* **1998**, *102*, 5898.
(17) Butkovskaya, N. I.; Setser, D. W. *J. Phys. Chem. A* **1998**, *102*, 9715.
(18) Meyer. S. T.; Temps, F. *Int. J. Chem. Kinet.* **2000**, *32*, 136.
(19) DeMore, W. B.; Sander, S. P.; Golden, D. M.; Hampson, R. F.; Kurylo, M. J.; Howard, C. J.; Ravishankara, A. R.; Kolb, C. E.; Molina, M. J., Jet Propulsion Laboratory Publication 97-4, Pasadena, CA, 1997.
(20) O'Keefe, A.; Deacon, D. A. G. *Rev. Sci. Instrum.* **1988**, *59*, 2544.
(21) Wheeler, N. D.; Newman, S. M.; Orr-Ewing, A. J.; Ashfold, M. N. R. *J. Chem. Soc., Faraday Trans.* **1998**, *94*, 337.
(22) Yu, T.; Lin, M. C. *J. Phys. Chem.* **1994**, *98*, 9697.
(23) Zhu, L.; Johnston, G. *J. Phys. Chem.* **1995**, *99*, 15114.
(24) Atkinson, D. B.; Hudgens, J. W. *J. Phys. Chem. A* **1997**, *101*, 3901.
(25) Atkinson, D. B.; Hudgens, J. W.; Orr-Ewing, A. J. *J. Phys. Chem. A* **1999**, *103*, 6173.
(26) Atkinson, D. B.; Hudgens, J. W. *J. Phys. Chem. A* **1999**, *103*, 4242.
(27) Ninomiya, Y.; Hashimoto, S.; Kawasaki, M.; Wallington, T. J. *Int. J. Chem. Kinet.* **2000**, *32*, 125
(28) Wallington, T. J.; Japar, S. M. *J. Atmos. Chem.* **1989**, *9*, 399.
(29) Zhu, L.; Kellis, D.; Ding, C. *Chem. Phys. Lett.* **1996**, *257*, 487.
(30) Japar, S. M.; Wallington, T. J.; Richert, J. F. O.; Ball. J. C. *Int. J. Chem. Kinet.* **1990**, *22*, 1257.
(31) Kaiser, E. W.; Wallington, T. J. *J. Phys. Chem.* **1994**, *98*, 5679.
(32) Niki, H.; Maker, P. D.; Breitenbach, L. P.; Savage, C. M. *Chem. Phys. Lett.* **1978**, *57*, 596.
(33) Pearson, J.; Orr-Ewing, A. J.; Ashfold, M. N. R.; Dixon, R. N. *J. Chem. Phys.* **1997**, *106*, 5850.
(34) (a) Becke, A. D. *Phys. Rev. A* **1988**, *38*, 3098. (b) Becke, A. D. *J. Chem. Phys.* **1993**, *98*, 5648.
(35) Lee, C.; Yang, W.; Parr, R. G. *Phys. Rev. B* **1988**, *37*, 785.
(36) Krishnan, R.; Binkley, J. S.; Seegar, R.; Pople, J. A. *J. Chem. Phys.* **1980**, *72*, 650.
(37) (a) Fukui, K. *J. Phys. Chem.* **1970**, *74*, 4161. (b) Fukui, K. *Acc. Chem. Res.* **1981**, *14*, 363.
(38) Frisch, M. J.; Trucks, G. W.; Schlegel, H. B.; Gill, P. M. W.; Johnson, B. G.; Robb, M. A.; Cheeseman, J. R.; Keith, T.; Petersson, G.

A.; Montgomery, J. A.; Raghavachari, K.; Al-Laham, M. A.; Zakrzewski, V. G.; Ortiz, J. V.; Foresman, J. B.; Cioslowski, J.; Stefanov, B. B.; Nanayakkara, A.; Challacombe, M.; Peng, C. Y.; Ayala, P. Y.; Chen, W.; Wong, M. W.; Andres, J. L.; Replogle, E. S.; Gomperts, R.; Martin, R. L.; Fox, D. J.; Binkley, J. S.; Defrees, D. J.; Baker, J.; Stewart, J. P.; Head-Gordon, M.; Gonzalez, C.; Pople, J. A. *Gaussian 94*, revision D4; Gaussian, Inc.: Pittsburgh, PA, 1995.

(39) (a) Abou-Rachid, H.; Pouchan, C.; Chaillet, M. *Chem. Phys*. **1984**, *90*, 243. (b) Kulkarni, S. A.; Koga, N. *J. Phys. Chem. A*, **1998**, *102*, 5228.

(40) Eyring, H.; Hirschfelder, J.; Taylor, H. *J. Chem. Phys.* **1936**, *4*, 479.

(41) (a) Robinson, P. J.; Holbrook, K. A. *Unimolecular Reactions*; Wiley: New York, 1972. (b) Forst, W. *Theory of Unimolecular Reactions*; Academic: New York, 1973.

(42) Troe, J. *J. Phys. Chem.* **1979**, *83*, 114.

(43) Gilbert, R. G.; Smith, S. C. *Theory of Unimolecular Recombination Reactions*; Blackwell Scientific Publication: Carlton, Australia, 1990.

(44) Hsu, C.-C.; Mebel, A. M.; Lin, M. C. *J Chem. Phys*. **1996**, *105*, 2346.

(45) Yamasaki, K.; Sato, M.; Itakura, A.; Watanabe, A.; Kakuda, T.; Tokue, I. Reactions of HCO ($\tilde{X}^2A'$, $\nu_1\nu_2\nu_3 = 000, 010, 001$) with Molecular Oxygen. *J. Phys. Chem. A*, in press.